Inositol monophosphatase regulates localization of synaptic components and behavior in the mature nervous system of *C. elegans*

Yoshinori Tanizawa,[1] Atsushi Kuhara,[1] Hitoshi Inada,[1,4] Eiji Kodama,[1] Takafumi Mizuno,[1] and Ikue Mori[1,2,3,5]

[1]Department of Molecular Biology, Division of Biological Science, Graduate School of Science, Nagoya University, Nagoya 464-8602, Japan; [2]Institute for Advanced Research, Nagoya University, Nagoya 464-8602, Japan; [3]PRESTO, Japan Science and Technology Corporation, Kawaguchi, Saitama 332-0012, Japan

Although recent studies have provided significant molecular insights into the establishment of neuronal polarity in vitro, evidence is lacking on the corresponding phenomena in vivo, including correct localization of synaptic components and the importance of this process for function of the nervous system as a whole. RIA interneurons act as a pivotal component of the neural circuit for thermotaxis behavior in the nematode *Caenorhabditis elegans* and provide a suitable model to investigate these issues, having a neurite clearly divided into pre- and post-synaptic regions. In a screen for thermotaxis mutants, we identified the gene *ttx-7*, which encodes *myo*-inositol monophosphatase (IMPase), an inositol-producing enzyme regarded as a bipolar disorder-relevant molecule for its lithium sensitivity. Here we show that mutations in *ttx-7* cause defects in thermotaxis behavior and localization of synaptic proteins in RIA neurons in vivo. Both behavioral and localization defects in *ttx-7* mutants were rescued by expression of IMPase in adults and by inositol application, and the same defects were mimicked by lithium treatment in wild-type animals. These results suggest that IMPase is required in central interneurons of the mature nervous system for correct localization of synaptic components and thus for normal behavior.

[*Keywords*: *C. elegans*; thermotaxis behavior; protein localization; synapse; *myo*-inositol monophosphatase; lithium]

Supplemental material is available at http://www.genesdev.org.

Received April 19, 2006; revised version accepted October 23, 2006.

Neurons are the most highly polarized animal cell type and are composed of several subcellular compartments, including axons, dendrites, and cell bodies, each of which has its own molecular and physiological characteristics. How these polarized compartments are established has been extensively investigated using cultured hippocampal neurons as a model system (Dotti and Banker 1987; Dotti et al. 1988). Recent studies have demonstrated that GSK-3β and small GTPase-mediated signaling pathways are critical in assigning axonal fate to the immature neurite in hippocampal neurons (Arimura and Kaibuchi 2005; Jiang et al. 2005). The established axonal compartment is physically separated from the cell body by a molecular diffusional barrier, which is at least partly responsible for maintaining the distinct character of these two compartments (Nakada et al. 2003). However, it remains to be determined whether these mechanisms are common to all neuronal types or other mechanisms exist as well. Furthermore, to understand the physiological importance of polarization and consequent subcellular heterogeneity such as localization of synaptic proteins, it is essential to evaluate how these subcellular phenomena in vivo correlate with the function of neurons and the nervous system as a whole.

The nematode *Caenorhabditis elegans* has a simple nervous system that consists of 302 neurons, the synaptic connectivity of which has been described in its entirety by electron microscopy (White et al. 1986). Although *C. elegans* neurons are less complex than those in vertebrates, many are similarly bipolar and have distinctive axons and dendrites, whose polarization mechanisms have recently begun to be clarified using genetics (Crump et al. 2001; Hallam et al. 2002). Other neurons are in a primitive unipolar form with a single neurite

[4]Present address: Center for Integrative Bioscience, National Institute for Physiological Sciences, Myodaiji, Okazaki 444-8787, Japan
[5]Corresponding author.
E-MAIL m46920a@nucc.cc.nagoya-u.ac.jp; FAX 81-52-789-4558.
Article is online at http://www.genesdev.org/cgi/doi/10.1101/gad.1497806.

that is both pre- and post-synaptic to its neighbors. Among these unipolar neurons, most of which have intermixed pre- and post-synaptic specializations within the neurite, RIA interneurons have the notable feature of a distinctive distal presynaptic region and proximal postsynaptic region within a single neurite (Fig. 3B, below; Supplementary Fig. S1A; White et al. 1986). This nearly complete separation of pre- and post-synaptic specializations in RIA neurites, combined with the ease of observing synapses in specific neurons labeled with fluorescent fusion proteins of synaptic proteins in *C. elegans* (Rongo et al. 1998; Nonet 1999; Yeh et al. 2005), provides a unique opportunity to analyze polarity establishment, synapse formation, and maintenance in vivo.

One of the major advantages of analyzing synapses in vivo in *C. elegans* is the ability to examine, through observation of behavior, how subcellular events affect function of the nervous system as a whole. RIA interneurons play an essential role in thermotaxis (TTX) behavior, in which *C. elegans* memorizes the ambient temperature in association with its feeding state and moves to that temperature when placed on a temperature gradient (Hedgecock and Russell 1975; Mori and Ohshima 1995; Mohri et al. 2005). Previous studies clarified that thermotaxis is governed by a neural circuit composed of thermosensory neurons, AFD, unidentified thermosensory neurons (indicated as X in Fig. 2C, below), and interneurons AIY, AIZ, and RIA (Fig. 2C, below; Mori and Ohshima 1995). It has been proposed that AFD and AIY neurons promote thermophilic behavior, AIZ neurons promote cryophilic behavior, and RIA neurons integrate signals from these upstream neurons. RIA neurons receive numerous synaptic inputs and emit outputs to downstream neurons that dominate the movement of neck muscles, thereby making the RIA neuron one of the most prominent integrative interneurons (White et al. 1986; Gray et al. 2005).

In this study, we show that TTX-7, the sole *C. elegans* ortholog of *myo*-inositol monophosphatase (IMPase; EC 3.1.3.25), controls localization of both of pre- and post-synaptic proteins within neurites of RIA interneurons and regulates sensory behaviors in the mature nervous system. IMPase is a lithium-sensitive enzyme that converts inositol monophosphates to inositol (Parthasarathy et al. 1994). IMPase is highly conserved among different species, including yeast, plants, and human. From its discovery in rat testis 40 yr ago (Eisenberg 1967), the structure and enzymatic properties of mammalian IMPase have been extensively investigated (Atack et al. 1995). Among many tissues expressing IMPase (McAllister et al. 1992), brain has attracted the most attention as a functional site of action, because inositol depletion through IMPase inhibition is proposed to be a possible underlying mechanism of lithium therapy for bipolar disorder (Berridge et al. 1989). Although exogenously applied lithium was reported to reduce the amount of inositol in rat brain (Allison and Stewart 1971), the relationship between the reduction of inositol and the therapeutic effect of lithium is still inconclusive because the actual site of lithium action in brain is unknown and lithium affects molecules other than IMPase (Lenox et al. 1998; Shaldubina et al. 2001; Jiang et al. 2005). Also, despite the strong emphasis on the critical role of IMPase in inositol production, IMPase is dispensable in yeast (Lopez et al. 1999), and other lithium-insensitive activities were found to dephosphorylate inositol monophosphates in *Dictyostelium* (Van Dijken et al. 1996). Thus, the function of IMPase in vivo remains largely unknown. The present study provides direct evidence that IMPase plays an important role in behavior and in localization of both pre- and post-synaptic proteins in RIA neurons, possibly by positively regulating inositol metabolism.

Results

ttx-7 *encodes an ortholog of* myo-*inositol monophosphatase*

To investigate the mechanisms of thermotaxis behavior, we conducted a genetic screen for thermotaxis-defective mutants, from which we isolated a novel mutant *ttx-7(nj40)*. Genetic mapping followed by transformation rescue revealed that the gene *ttx-7* was identical to the predicted gene F13G3.5 (Fig. 1A). Analysis of cDNA clones showed that F13G3.5 encodes two splice isoforms that we designated *ttx-7a* and *ttx-7b*, differing in an alternative fifth exon (Fig. 1B). Because nine of 10 available cDNA clones encoded *ttx-7a*, and because the rescuing activity of *ttx-7b* was much lower than that of *ttx-7a* (data not shown), we concluded that *ttx-7a* is the major isoform and thus used only *ttx-7a* cDNA in this study.

The predicted peptide sequence of TTX-7A showed 45.6% identity to human IMPase 1 over its entire length, suggesting that TTX-7 is an ortholog of IMPase. Studies on mammalian IMPases revealed the key amino acid residues important for the activity of IMPase, which are all conserved in TTX-7 (Fig. 1C; Atack et al. 1995). The *ttx-7* genomic clone with a substitution in one of the key residues (D99N in TTX-7, corresponding to D93N in human IMPA1; Pollack et al. 1993) could not rescue the thermotaxis defect of *ttx-7* mutants, suggesting that TTX-7 shares common enzymatic properties with its mammalian counterpart (data not shown). A Blast search of genes in the *C. elegans* genome against human IMPases revealed no other *C. elegans* gene as highly homologous to IMPases as TTX-7 (Supplementary Table S1). These results suggest that TTX-7 is the sole *C. elegans* ortholog of IMPase in contrast to other organisms that have multiple IMPase homologs (Fig. 1D).

Sequencing the *ttx-7(nj40)* genome revealed that *nj40* is a missense mutation of the conserved glycine residue whose role is unknown (Fig. 1C). As *nj40* might represent a weak allele, we additionally isolated two deletion mutants *ttx-7(nj50)* and *ttx-7(nj51)* from our mutant bank created by TMP/UV mutagenesis (Gengyo-Ando and Mitani 2000; N. Nishio, H. Inada, and I. Mori, unpubl.). Both of the two deletion mutants are likely null, because *nj50* lacks the first exon, including the initial methionine, and *nj51* lacks the third exon, including

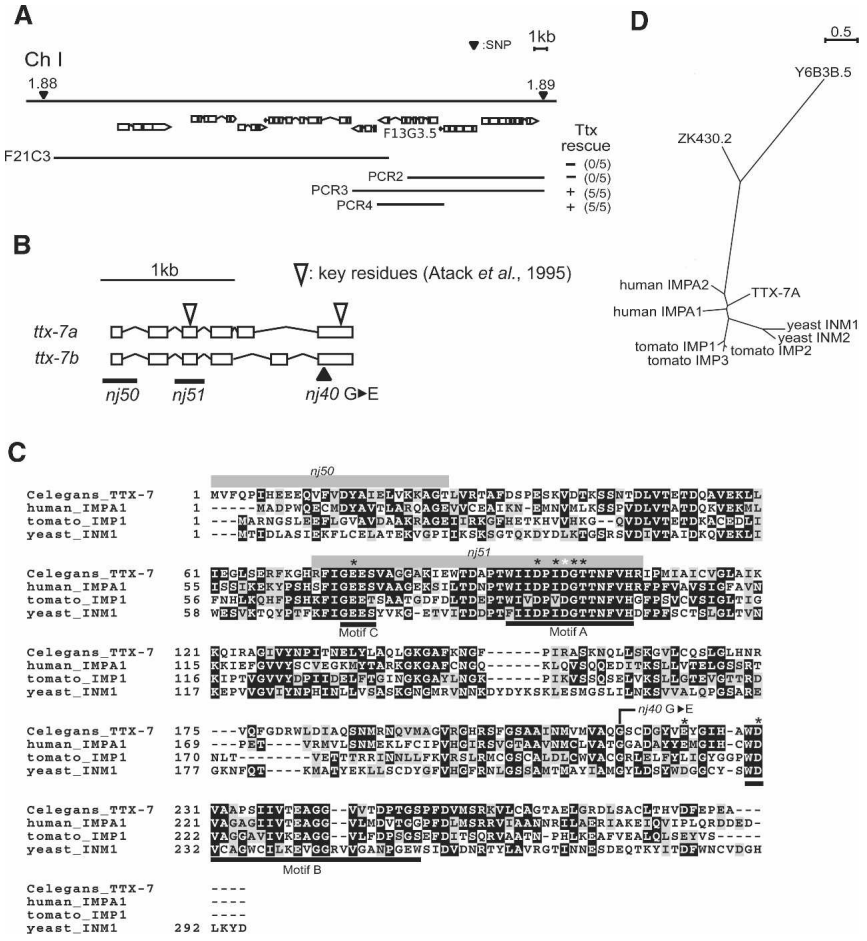

Figure 1. Genetic and molecular analyses of *ttx-7*. (*A*) Position of *ttx-7* on chromosome I. *ttx-7* was mapped between two SNPs. Results of rescue experiments for *ttx-7* mutant thermotaxis defects are indicated as + (rescued) or – (not rescued). The numbers in parentheses are the fraction of rescued lines. (*B*) Two types of cDNA clones. Exons are boxed, and key residues are indicated by open triangles (Atack et al. 1995). Mutation sites of *ttx-7* mutants are illustrated. (*C*) Comparison of sequences of TTX-7A and IMPases in other species. Black and gray boxes highlight identical and similar residues, respectively. Black bars *below* the sequences indicate conserved motifs, and asterisks indicate key residues (Atack et al. 1995). The aspartate with a white asterisk is the residue whose conversion to asparagine abolished the enzymatic activity of TTX-7 (see text). Deletions are indicated by gray bars *above* the sequences. (*D*) Phylogenic analysis of full-length sequences of IMPase orthologs and two other *C. elegans* proteins, ZK430.2 and Y6B3B.5, that have less similarity to human IMPases than TTX-7 (Supplementary Table S2). The dendrogram was generated with ClustalW and NJplot.

many of the residues important for enzymatic activity of IMPase (Fig. 1B,C; Atack et al. 1995). All three mutations were recessive for the thermotaxis and presynaptic phenotypes described below (data not shown; not determined for other phenotypes). We mainly used *nj50* in this study.

TTX-7/IMPase is expressed strongly in subsets of neurons

To determine its site of action, we analyzed the expression pattern of *ttx-7* fused with EGFP, which completely rescued the thermotaxis defects of *ttx-7* mutants (Fig. 2A; data not shown). Strong and consistent expression was observed in a limited number of neurons in the head and tail and coelomocytes (Fig. 2B). Consistent with this result, mammalian IMPase is strongly expressed in the nervous system (McAllister et al. 1992). Weaker and/or inconsistent expression of TTX-7::EGFP was detected in nerve cord motor neurons, intestine, and somatic gonad (Fig. 2B; data not shown). TTX-7::EGFP was diffusely expressed in the cytoplasm and was not localized to any specific subcellular compartment. We identified most of the head neurons expressing *ttx-7*::EGFP (Fig. 2B), of which AFD and RIA neurons are components of the thermotaxis neural circuit (Fig. 2C).

RIA neurons of ttx-7 *mutants have no severe morphological defects*

As TTX-7 was demonstrated to function in RIA neurons (discussed below), we examined whether RIA neurons have any cell biological defects. As illustrated in Figure 3A, each of the left/right counterparts of RIA neurons has its cell body in the lateral ganglia of the head and sends a single neurite to the nerve ring. We first observed the overall morphology of RIA neurons by expressing GFP as a soluble marker using an RIA-specific promoter. Although swellings and tiny protrusions were observed more often in *ttx-7* mutants than in wild-type animals, no other severe morphological defect was observed (Fig. 3C). Because the expression level of GFP was similar between wild-type and *ttx-7* animals (Fig. 3C; data not shown), the regulation of gene expression also appeared intact in this mutant.

To further characterize general structural features of RIA neurons, we expressed YFP-GPI, a membrane-anchored YFP, in RIA neurons (Rolls et al. 2002). In wild-type animals, YFP-GPI localized diffusely on the plasma membrane, and punctate intracellular structures were visualized in the cell body (Fig. 3C). In neurites, fluorescence in the distal region was slightly but significantly brighter compared with the proximal region, which

might reflect localization of YFP-GPI on the membrane of synaptic vesicles that are abundant in the distal region (see below; Fig. 3C; Supplementary Fig. S1B). In the *ttx-7* mutant RIA cell body, YFP-GPI often localized on internal membranous structures in addition to the plasma membrane (Supplementary Fig. S1C). Membrane swellings were more often observed in *ttx-7* mutants, as seen with soluble GFP, but there was no difference in distribution of YFP-GPI in RIA neurites between wild-type animals and *ttx-7* mutants (Fig. 3C; Supplementary Fig. S1B). These results suggest that *ttx-7* mutants have no severe morphological defects in RIA neurites at light-microscopic resolution.

Synaptic proteins localize abnormally in RIA neurons of ttx-7 *mutants*

As White and colleagues described (White et al. 1986), RIA neurites have numerous chemical synapses (Supplementary Table S2). Notably, all of the presynaptic specializations are located in the distal region of the neurite, whereas most of the post-synaptic specializations are lo-

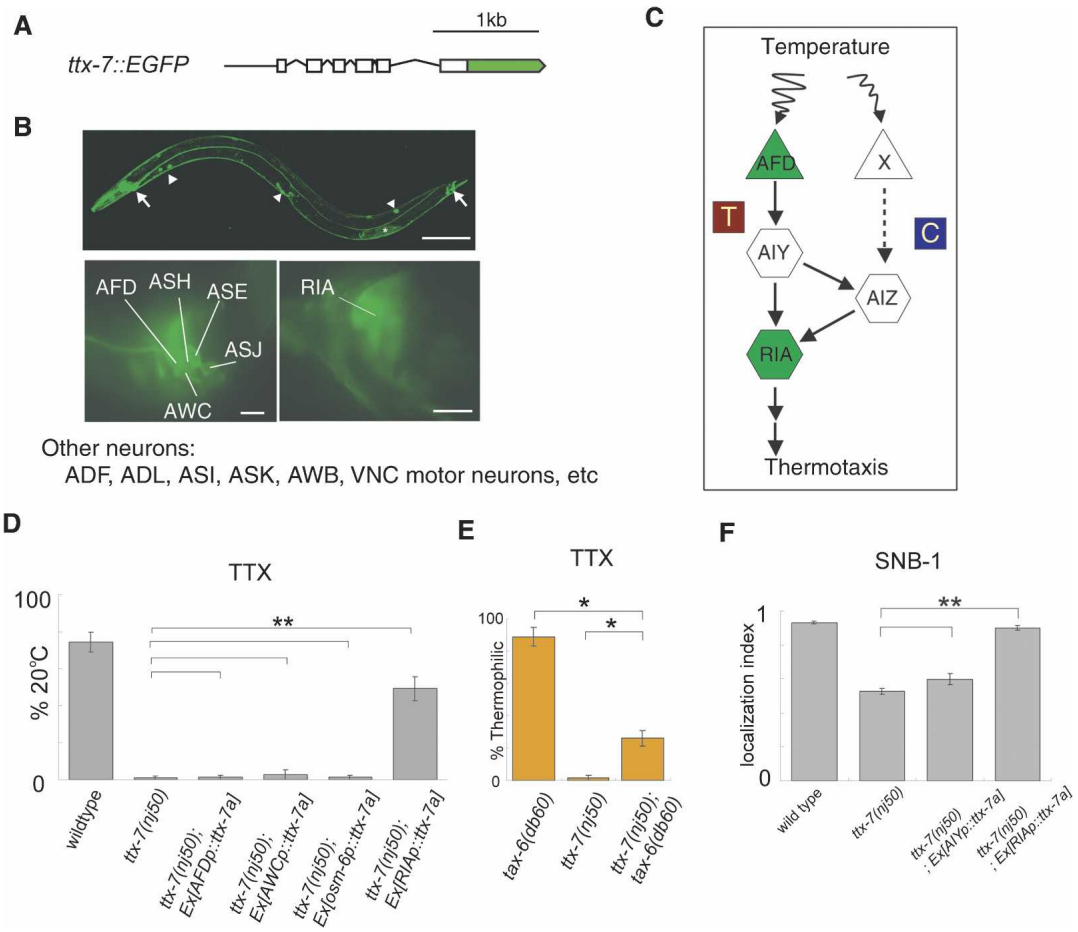

Figure 2. Expression pattern and cell-autonomous function of TTX-7 in RIA neurons. (*A*) The *ttx-7*::EGFP fusion gene. (*B*) Expression of *ttx-7*::EGFP. Anterior is to the left, dorsal is up. (*Top* panel) Strong fluorescence was observed in head and tail neurons (arrow) and coelomocytes (arrowhead). Bar, 100 µm. (*Bottom left* panel) In the head, a limited number of neurons express *ttx-7*::EGFP. Bar, 5 µm. (*Bottom right* panel) Expression in RIA neurons was observed in another focal plane. Bar, 5 µm. Other identified neurons are listed in the figure. (*C*) The proposed thermotaxis neural circuit (Mori and Ohshima 1995). AFD is a major thermosensory neuron, and X is a putative minor thermosensory neuron. AFD and AIY neurons promote thermophilic behavior (indicated as "T"), and AIZ neurons promote cryophilic behavior (indicated as "C"). RIA neurons are proposed to integrate these signals. In this circuit, AFD and RIA express *ttx-7* and are colored green. (*D*) Cell-specific rescue of the thermotaxis defect in *ttx-7* mutants by *ttx-7a* cDNA expression. Bars show the percentage of animals that moved to the cultivation temperature (20°C). *osm-6p* induces expression in many sensory neurons. Compared with naïve *ttx-7* mutants, only transgenic strains with *RIAp*::*ttx-7a* showed improved thermotaxis (Dunnett's multiple comparison test; $n = 3$ or more assays). (*E*) Genetic epistasis of *ttx-7* and *tax-6* mutants in thermotaxis. Note that the bars indicate the percentage of thermophilic animals. The *ttx-7* mutation suppressed the thermophilic behavior of *tax-6* mutants, but the double mutants were still more thermophilic than *ttx-7* mutants (Dunnett's multiple comparison test; $n = 4$ or more assays). (*F*) Cell-specific rescue of the SNB-1 localization defect in *ttx-7* mutants. Localization indexes were calculated as shown in Figure 3B and Materials and Methods. The localization was rescued not with *AIYp*::*ttx-7a* but with *RIAp*::*ttx-7a* (Steel's multiple comparison test; $n = 10$ animals).

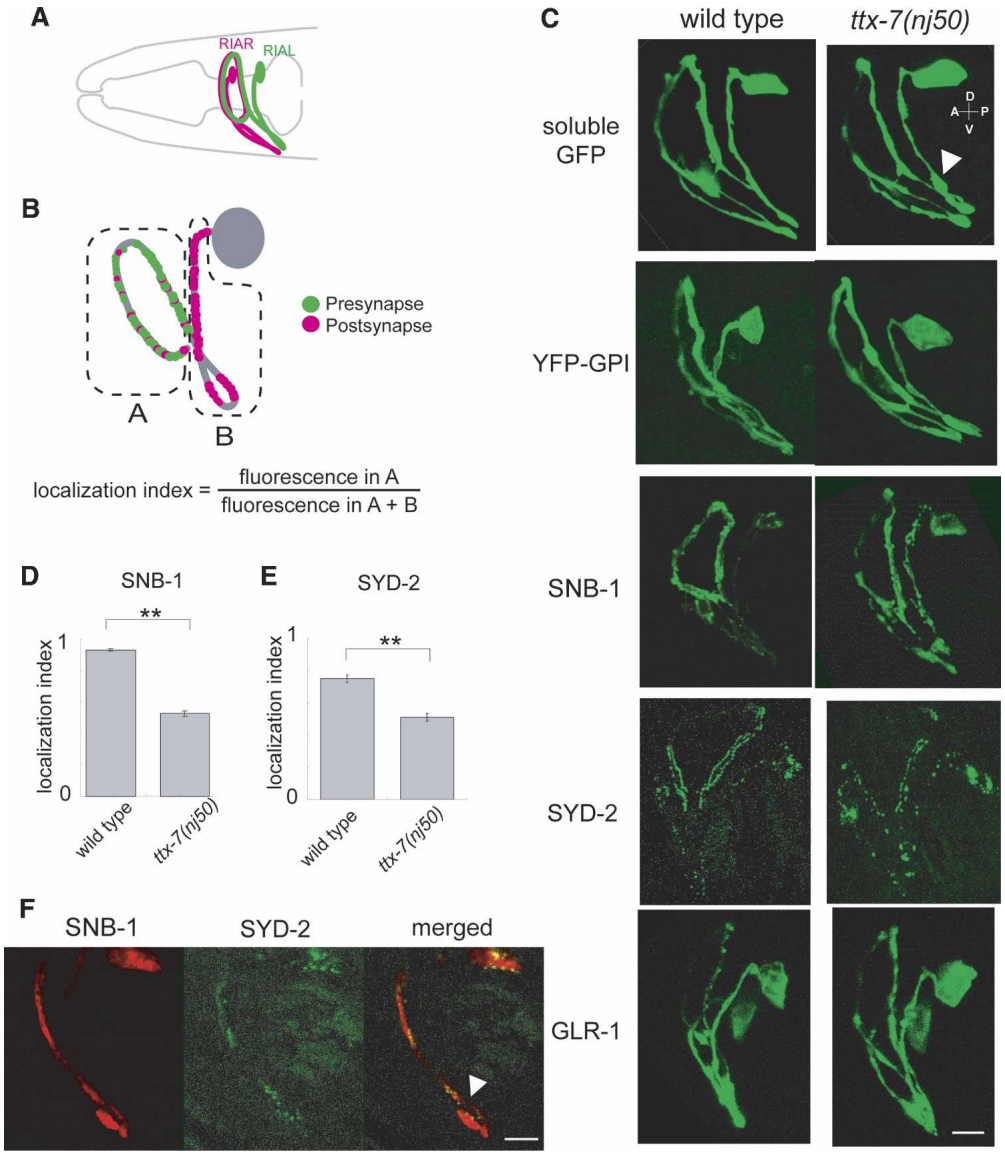

Figure 3. Synaptic defects in RIA neurons. (*A*) Schematic drawing of the head region. Colored circles and lines represent cell bodies and neurites of RIA neurons, respectively. Left (green) and right (magenta) counterparts, whose neurites overlap in their distal regions, are illustrated. Anterior is to the left, dorsal is up. (*B*) Schematic drawing of synapse distribution in an RIA neuron (White et al. 1986), and calculation of the localization index. Presynapses and post-synapses are indicated in green and magenta, respectively. Fluorescence intensity in regions A (distal neurite) and B (isthmus and proximal neurite) are measured and used to calculate the localization index with the formula described in Materials and Methods. A single RIA neuron is illustrated for simplicity. (*C*) Fluorescence images of RIA neurons in wild-type and *ttx-7* animals. (First row) RIA neurons expressing soluble GFP. In *ttx-7* mutants, minor swellings in the neurite were observed more often than in wild type (arrowhead). (Second row) RIA neurons expressing YFP-GPI. (Third row) RIA neurons expressing SNB-1::VENUS. (Fourth row) RIA neurons expressing GFP::SYD-2. (Fifth row) RIA neurons expressing GLR-1::GFP. Bar, 5 µm. (*D*) Localization indexes of SNB-1::VENUS. *ttx-7* mutants showed a lower index than wild-type animals (Mann-Whitney U-test; $n = 11$ for wild type, $n = 10$ for *ttx-7*). (*E*) Localization indexes of GFP::SYD-2 are also lower in *ttx-7* mutants than in wild-type animals (Mann-Whitney U-test) ($n = 20$ animals). (*F*) Localization of SNB-1::ECFP (*left*) and GFP::SYD-2 (*middle*) in *ttx-7* mutants were simultaneously visualized. (*Right* panel) Both were often observed to accumulate in the distal end of the post-synaptic region (arrowhead). Dorsal is up, anterior is to the left. Bar, 5 µm.

cated in the proximal region; these two regions are connected by an isthmus-like structure devoid of synapses (Fig. 3B,C; for ventral view, Supplementary Fig. S1A). Thus, the apparent monopolar neurite of the RIA neuron is in fact bipolar in terms of the separation of distal presynaptic and proximal post-synaptic regions within it.

To gain insight into the intracellular state of RIA neurons, we observed localization of synaptic proteins by expressing them as fluorescent protein-tagged fusions using an RIA-specific promoter.

We observed the localization of SNB-1, the synaptic vesicle protein synaptobrevin, in RIA neurons. In wild-

type animals, SNB-1 tagged with VENUS localized exclusively in the presynaptic region and appeared punctate, implying that SNB-1 correctly localized on presynaptic vesicles. In contrast, SNB-1 mislocalized over the entire length of the neurite in *ttx-7* mutants (Fig. 3C; Supplementary Fig. S1E). When quantified as shown in Figure 3B, the localization index for SNB-1 fluorescence distribution differed significantly between wild-type and *ttx-7* animals (Fig. 3D). In contrast, the localization index calculated by the same formula using the fluorescence intensity of soluble GFP was similar between wild-type and mutant animals, excluding the possibility that neurite volume itself changed in *ttx-7* mutants (Supplementary Fig. S1B). Similar control experiments were performed using soluble GFP in subsequent localization measurements (see below; Supplementary Fig. S1B), and no significant changes were detected. Because different synaptic vesicle proteins are in some cases transported via alternate mechanisms (Nonet et al. 1999), we examined the localization of another synaptic vesicle protein, SNG-1/synaptogyrin, tagged with GFP. SNG-1 mislocalized in the same way as SNB-1 in *ttx-7* mutants (Supplementary Fig. S1D). These results suggest that *ttx-7* mutants have general defects in localization of synaptic vesicle proteins.

Mislocalization of synaptic vesicle proteins implies that a more fundamental process may be defective in *ttx-7* mutants. To verify this hypothesis, presynaptic active zones were observed with two additional GFP-tagged proteins: SYD-2, the active zone protein α-liprin (Yeh et al. 2005), and highwire/PAM encoded by *rpm-1*, a periactive zone protein that regulates synaptogenesis (Zhen et al. 2000). When expressed in RIA neurons of wild-type animals, SYD-2 localized exclusively to the presynaptic region and appeared punctate, implicating localization to presynapses (Fig. 3C). In *ttx-7* mutants, the fluorescence was dimmer in the presynaptic region and brighter outside of it, resulting in a lower localization index than in wild-type animals (Fig. 3C,E). Likewise, RPM-1 tagged with GFP mislocalized outside of the presynaptic region in *ttx-7* mutants, though its fluorescence was too dim to photograph (data not shown).

Finally, we visualized post-synaptic specializations with GFP-tagged GLR-1, a non-NMDA-type ionotropic glutamate receptor (Rongo et al. 1998). In contrast to presynaptic components, GLR-1::GFP expressed in RIA neurons of wild-type animals localized mainly in the proximal region of the neurite, which is exclusively postsynaptic. Dispersed fluorescent spots were observed in the distal region, which is consistent with the observation that several post-synapses exist there (Fig. 3C; White et al. 1986). When expressed in *ttx-7* mutants, GLR-1::GFP mislocalized throughout the neurite, with considerable fluorescence detected also in the distal, mainly presynaptic region (Fig. 3C).

In summary, our observations using fluorescence-tagged synaptic proteins reveal that loss of TTX-7 function causes mislocalization of synaptic proteins in general, without resulting in severe morphological defects in RIA neurites.

Presynaptic proteins mislocalize randomly by an unknown mechanism

To determine if the mislocalized synaptic proteins localized randomly or constituted ectopic synaptic specializations in *ttx-7* mutants, we examined whether mislocalized SNB-1 and SYD-2 colocalized in the proximal region of the neurite. As shown in Figure 3F, ECFP-tagged SNB-1 mislocalized over the entire proximal region, whereas GFP-tagged SYD-2 showed scattered distribution along the neurite with most of the label not colocalized with SNB-1 spots. Although they both often accumulated in the distal end of the proximal region next to the isthmus (Fig. 3F, arrowhead), we could not determine whether they colocalized and made ectopic synapses there due to the high density of fluorescent spots.

Because IMPase is known as an inositol-producing enzyme and inositol-containing lipids are important regulators of membrane cycling (Cremona and De Camilli 2001), we speculated that synaptic protein localization defects in *ttx-7* mutants are caused by a failure of membrane cycling. Thus, we screened available mutants whose mutations abolish inositol metabolism, inositol signaling, or synaptic vesicle cycling, in search for possible downstream components of TTX-7/IMPase. As summarized in Supplementary Table S3, some mutants showed less dramatic SNB-1 mislocalization in RIA neurons than that observed in *ttx-7* mutants (Supplementary Fig. S2A). Of those, the *unc-11* mutant, which lacks the function of the AP180 homolog important for endocytosis (Nonet et al. 1999), showed the most severe mislocalization. The appearance of SNB-1 localization in *unc-11* mutants, however, appeared diffuse on the plasma membrane, which differed from the punctuate appearance in *ttx-7* mutants (Fig. 3C; Supplementary Fig. S2A), suggesting that their actions also differ as supported by the additive phenotype in *unc-11 ttx-7* double mutants (Supplementary Fig. S2A). The supposition that localization defects in *ttx-7* mutants are not simply caused by endocytosis defects was further supported by the different appearance of wild-type SNB-1 localization in *ttx-7* mutants compared with that of the endocytosis-defective mutant SNB-1 (M38A) in wild-type animals, which is known to localize on the plasma membrane (Supplementary Fig. S2B; Grote and Kelly 1996). These results suggest that synaptic components mislocalized randomly in RIA neurons of *ttx-7* mutants and that the cause of the defects cannot be explained simply by a single disruption of known vesicle cycling or inositol metabolism steps.

ttx-7 *mutants show severe defects in sensory behaviors*

To characterize behavior in *ttx-7* mutants, we conducted several sensory and other behavioral assays. In the thermotaxis assay, wild-type animals cultivated at 20°C moved normally to the cultivation temperature. In contrast, *ttx-7(nj40)*, *ttx-7(nj50)*, and *ttx-7(nj51)* mutants showed a severe athermotactic defect (Fig. 4A,B). *ttx-7*

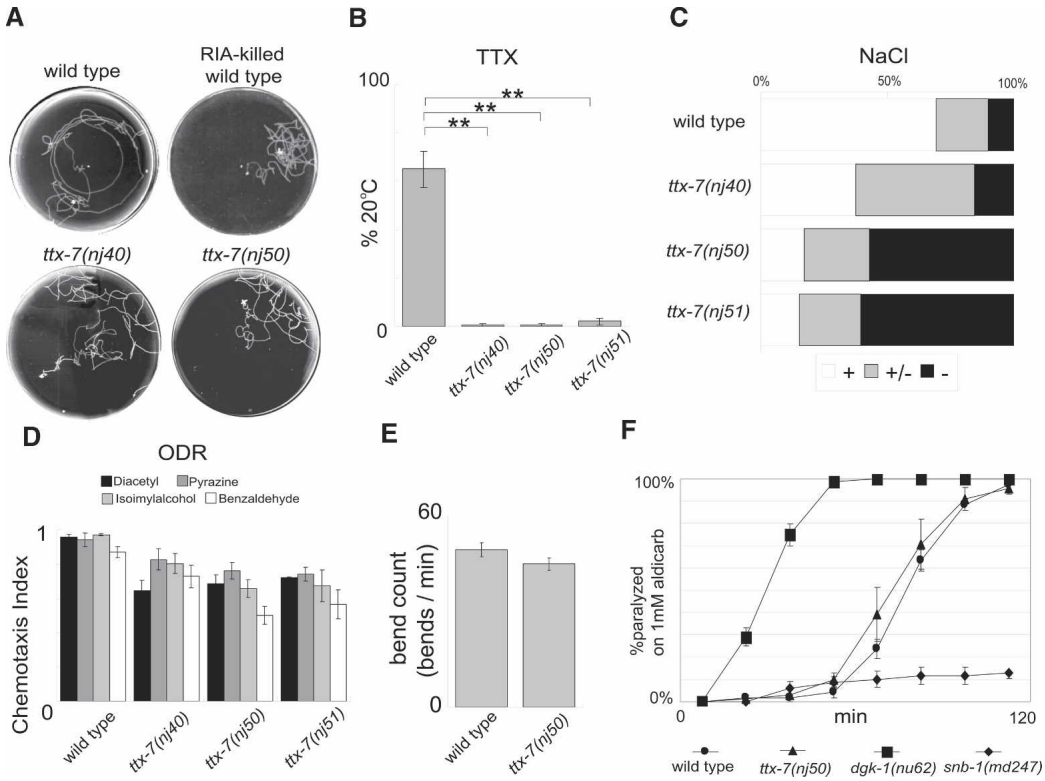

Figure 4. Behavioral defects in *ttx-7* mutants. (*A*) Thermotaxis tracks of naïve wild-type, RIA-killed wild-type, and *ttx-7* animals after cultivation at 20°C. A radial thermal gradient was established on the assay plates, which was 17°C at the center and 25°C at the periphery. (*B*) Thermotaxis assay. Bars indicate the percentage of animals that moved to the cultivation temperature, 20°C, on the assay plates ($n \geq 4$ assays). Dunnett's multiple comparison test was performed. (*C*) Chemotaxis to the soluble attractant NaCl. (+) Strong attraction; (+/−) moderate attraction; (−) no attraction. No difference between wild type and *ttx-7* mutants was observed. $n = 60$ animals. (*D*) Chemotaxis to volatile attractants. Bars show the chemotaxis index indicating the extent of attraction, which did not differ significantly between wild type and *ttx-7*. $n = 3$ or more assays. (*E*) Bend counts per minute did not differ significantly between wild type and *ttx-7* (Mann-Whitney U-test; $n = 10$ animals). (*F*) Sensitivity to aldicarb (1 mM). The graph shows the percentage of animals paralyzed at the time indicated. The EC50 values calculated with Origin software did not differ significantly between wild-type and *ttx-7* animals (Student's *t*-test; $n = 3$ assays, 25 animals assayed per strain).

mutants showed similar athermotactic defects when cultivated at other temperatures, which indicates that *ttx-7* mutants have athermotactic defects that are mostly independent of the cultivation temperature (Supplementary Fig. S3A). *ttx-7(nj50)* and *ttx-7(nj51)* were more defective in chemotaxis than *ttx-7(nj40)* mutants (Fig. 4C,D), suggesting that *nj40* is a hypomorphic allele.

As *ttx-7* is expressed in motor neurons (Fig. 2B), we conducted assays to examine the motor activity of *ttx-7* mutants. First, we counted body bends per minute and found that *ttx-7* mutants showed a tendency to bend less frequently than wild-type animals, but the difference did not reach statistical significance (Fig. 4E). In another assay, we cultivated animals on plates containing the acetylcholinesterase inhibitor aldicarb and counted the percentage of animals that became paralyzed (Fig. 4F). We could not find any difference in sensitivity to aldicarb between wild-type and mutants, consistent with the reported result with RNA interference (RNAi)-treated animals (Sieburth et al. 2005). These results show that motor activity in *ttx-7* mutants is largely intact.

The inositol trisphosphate (IP3) receptor plays an important role in defecation and egg laying behavior in *C. elegans* (Dal Santo et al. 1999). Because IMPase has been regarded as a key enzyme in inositol production and the IP3 receptor is activated by the inositol-derivative IP3, we examined whether *ttx-7* mutants showed defects in these behaviors. Unexpectedly, *ttx-7* mutants showed only slightly reduced brood size (243.2 ± 11.3 [SEM]; $n = 10$) compared with wild-type animals (279.3 ± 8.2 [SEM]; $n = 12$) ($p < 0.05$, Mann-Whitney's U-test) and had similar defecation cycles: 45.4 ± 0.93 (SEM) sec ($n = 5$) for wild-type and 44.7 ± 0.69 (SEM) sec ($n = 5$) for *ttx-7(nj50)* animals (Student's *t*-test). These results stand in contrast to the severe phenotypes reported for IP3 signaling mutants (Dal Santo et al. 1999), and suggest that loss of TTX-7/IMPase has little effect on many aspects of inositol signaling in *C. elegans*, significantly impacting only specific functions such as sensory behaviors.

TTX-7 acts cell autonomously in RIA interneurons

To determine in which cell type TTX-7 acts for synaptic protein localization and thermotaxis behavior, we con-

ducted cell-specific rescue experiments of *ttx-7* mutants by introducing *ttx-7a* cDNA driven by cell-specific promoters. As shown in Figure 2D, expression of *ttx-7a* cDNA in RIA neurons rescued the thermotaxis defect of *ttx-7* mutants. Although the rescue was not complete in these transgenic animals, we could not find any other neurons in which expression of *ttx-7a* cDNA additionally improved thermotaxis behavior. RIA-specific expression of *ttx-7a* cDNA also rescued SNB-1 mislocalization in RIA neurons (Fig. 2F). These results suggest that TTX-7 acts cell autonomously in RIA neurons for both synaptic protein localization and thermotaxis.

To elucidate to what extent TTX-7 is essential for RIA neurons to function normally during thermotaxis, we compared the thermotaxis defect of *ttx-7* mutants with that of RIA-killed wild-type animals and found that their thermotaxis phenotypes highly resembled one another (Fig. 4A; Supplementary Fig. S3B; Mori and Ohshima 1995). This result further supports our conclusion that TTX-7 acts in RIA neurons and suggests that the function of RIA neurons is strongly abolished in *ttx-7* mutants.

If RIA neurons are indeed pivotal integrative components in the thermotaxis neural circuit as proposed (Fig. 2C; Mori and Ohshima 1995), then disruption of RIA function should eliminate any signaling from upstream neurons. To test this hypothesis, we used the *ttx-7* mutation as a tool to ablate RIA neurons genetically. In *tax-6* mutants, AFD neurons are hyperactivated and send activated signals downstream to induce thermophilic behavior (Kuhara et al. 2002). The double mutants *ttx-7; tax-6* showed athermotactic behavior similar to *ttx-7* single mutants, demonstrating that genetic ablation of RIA neurons strongly suppresses a hyperactivated signal from upstream thermosensory neurons, which supports the proposed thermotaxis neural circuit (Fig. 2E).

TTX-7 is required in the mature nervous system

To specify when TTX-7 functions, we induced expression of *ttx-7a* cDNA in *ttx-7* mutants at specific developmental stages using the heat-shock promoter and observed the phenotypes of treated animals at adult stages. Little rescue of thermotaxis defects was observed when heat shock was applied at or before larval stages. In contrast, heat shock in the adult stage rescued the thermotaxis defect (Fig. 5A,B). Heat shock at adult stages could also rescue SNB-1 and SYD-2 localization defects (Fig. 5A,C,D). These results suggest that adult-stage-restricted expression of *ttx-7* is sufficient for its function and that a large portion of the defects in *ttx-7* mutants is not developmentally irreversible. In addition, when ani-

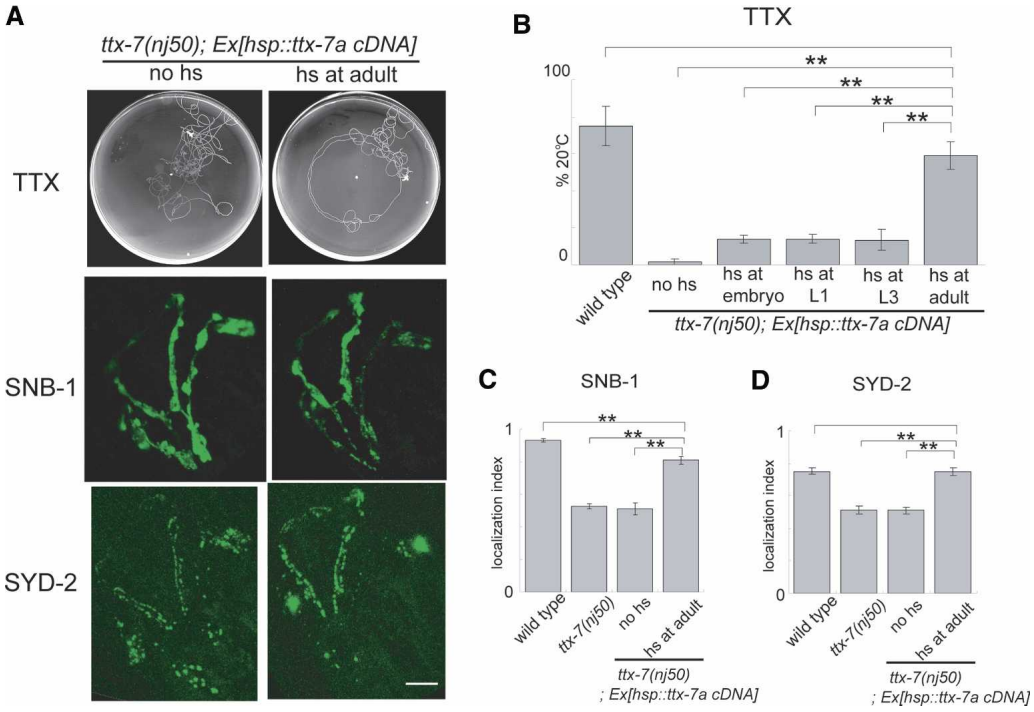

Figure 5. Rescue of defects by adult-stage-specific expression of *ttx-7*. (*A*) Thermotaxis tracks and synaptic protein localization in *ttx-7* mutants with transgene *hsp16-2p*::*ttx-7a* cDNA. Animals had not been (no hs) or had been (hs at adult) exposed to heat shock at the adult stage. (*B*) Heat-shock rescue of thermotaxis. *ttx-7* mutants with the transgene were exposed to heat shock at the stages indicated and were assayed as adults. *ttx-7* mutants without the transgene were not rescued by heat shock (data not shown) (Dunnett's multiple comparison test; $n = 3$ assays). (*C*) Localization indexes of SNB-1::VENUS in heat-shock experiments. TTX-7 expression in adult stages rescued SNB-1 localization, although the index of rescued animals was still lower than that of wild-type animals (Steel's multiple comparison test; $n = 10$ animals). (*D*) Localization indexes of GFP::SYD-2 in heat-shock experiments. TTX-7 expression at the adult stage rescued SYD-2 localization in *ttx-7* mutants (Steel's multiple comparison test; $n = 10$–20 animals).

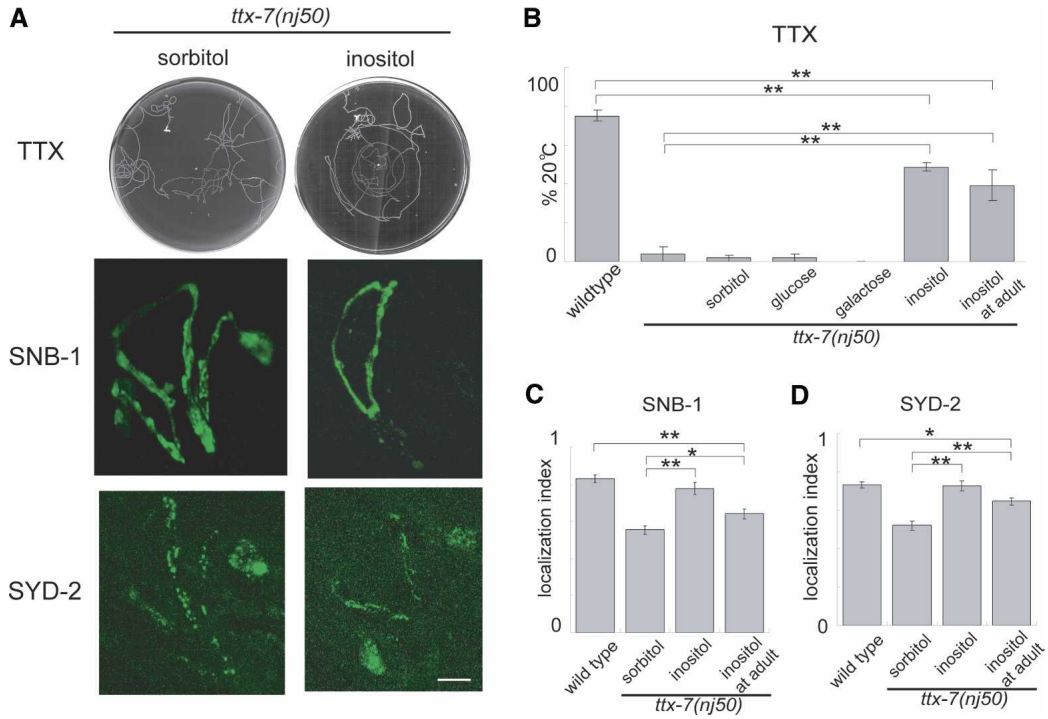

Figure 6. Effects of exogenously applied inositol. (*A*) Thermotaxis tracks and protein localization in RIA neurons of *ttx-7* mutants grown from birth with sorbitol or inositol. (*B*) Effects of inositol and other monosaccharides on thermotaxis behavior of *ttx-7* mutant animals. "Inositol at adult" indicates that animals were treated with inositol after they grew to be adults, whereas animals in the other conditions were cultivated under constant conditions (see text). Although not illustrated for simplicity, the difference between wild-type and the other groups, and the difference between each of the two *right*-most treatments and each of sorbitol, glucose, and galactose treatments, were also significant ($p < 0.01$, Tukey's multiple comparison test; $n \geq 3$ assays). (*C,D*) Localization index of SNB-1::VENUS and GFP::SYD-2 in animals grown with monosaccharides. Inositol application in the adult stage rescued the indexes of *ttx-7* mutants, which were still lower than that of wild-type animals (Steel-Dwass multiple comparison test; $n = 10$ or more animals).

mals were heat-shocked for various periods, there was a positive correlation between the extent of rescue of localization and behavioral phenotypes (Supplementary Fig. S4A–C), indicating a close relationship between synaptic protein localization and behavior.

Inositol rescues defects in ttx-7 *mutants*

Because IMPase is an inositol-producing enzyme, inositol shortage caused by loss of TTX-7/IMPase might account for the defects in *ttx-7* mutants. After *ttx-7* mutants were grown from birth in the presence of inositol, both thermotaxis and localization defects were significantly rescued (Fig. 6A–D). The rescuing activity was specific to inositol, because the other monosaccharides of the same atomic composition did not rescue the defects. Furthermore, applying inositol only in adult stages rescued the defects (Fig. 6B–D), which is consistent with the result of the heat-shock-induced rescue experiments. These results suggest that TTX-7 is required to supply inositol, which also indicates that TTX-7 actually acts as an inositol-producing IMPase in vivo. We also found that galactose delayed the development of *ttx-7* mutants, but not of wild-type animals, which might suggest that IMPase also acts in galactose metabolism (Parthasarathy et al. 1997).

The IMPase inhibitor lithium reversibly mimics TTX-7 disruption

We next investigated whether exogenous application of lithium chloride (LiCl), a potent inhibitor of IMPase in vitro, to wild-type animals could mimic the loss of TTX-7. Although cultivation with LiCl from birth often caused concentration-dependent developmental retardation and partial movement defects (data not shown), in the behavioral assays shown here we used treated animals that grew and moved normally. As shown in Figure 7A and Supplementary Fig. S5D–F, cultivation with 15 mM LiCl from birth caused thermotaxis and synaptic localization defects in wild-type animals, similar to *ttx-7* mutants. Thus, treatment with LiCl from birth completely mimicked the phenotypes of *ttx-7* mutants.

To determine whether adult-stage-specific inhibition of TTX-7 is enough to mimic the disruption of *ttx-7*, we applied LiCl to adult wild-type animals. After overnight cultivation in 15 mM LiCl, adult wild-type animals showed as severe thermotaxis defect as *ttx-7* mutants

(Fig. 7A,E; Supplementary Fig. S5G). Although the same treatment did not cause as severe localization defects as observed in *ttx-7* mutants, the effects were clearly observed: Overnight LiCl reduced the amount of SYD-2 in the presynaptic region (2804 ± 327 [SEM] A.U. for untreated animals and 899 ± 129 [SEM] A.U. for LiCl-treated animals, $p < 0.01$, Mann-Whitney U-test) (Fig. 7A), and in a portion of the treated animals caused mislocalization of SNB-1 similar to that observed in *ttx-7* mutants (29.1 ± 2.46% for treated and 0% for untreated animals) (Fig. 7A). Thus, application of LiCl to adults mimicked the effects of *ttx-7* disruption partially but significantly for synaptic localization and completely for thermotaxis. Intriguingly, the disrupted behavior and lo-

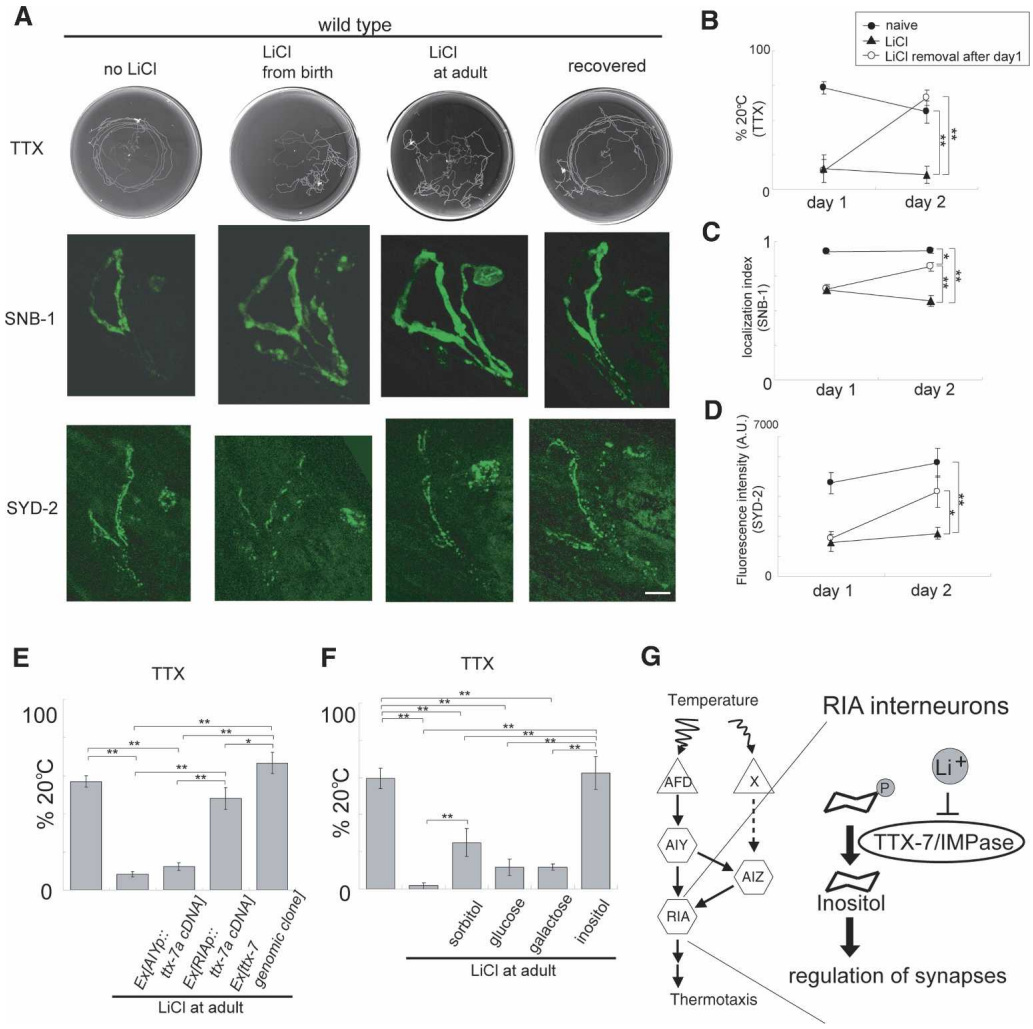

Figure 7. Effects of exogenously applied LiCl. (*A*) LiCl reversibly disrupts thermotaxis and protein localization. (First row) Thermotaxis. (Second row) SNB-1 localization. (Third row) SYD-2 localization. In each row, wild-type animals that were cultivated without LiCl, (first column) with LiCl from birth (second column), and with LiCl overnight after cultivation without LiCl to adulthood (third column) are shown. (Fourth column) The individuals shown in the third column were cultivated one more day without LiCl and observed again. For quantification for the experiments shown in the second column, see Supplementary Figure S5D–F. (*B–D*) Overnight LiCl-induced defects are reversible. Filled circles and filled triangles indicate naïve and continuously LiCl-treated wild-type animals, respectively. Open circles indicate the animals that had been cultivated overnight with LiCl until the first observation on day 1 and thereafter cultivated without LiCl until the second observation on day 2. Statistical analyses were performed on the data for day 2 with Tukey's (*B*) or Steel-Dwass (*C*,*D*) multiple comparison test. (*B*) Thermotaxis ($n = 3$ assays). (*C*) SNB-1 localization index ($n = 10$ animals). (*D*) Fluorescence intensity of GFP::SYD-2 in the distal region of the neurite. The localization index could not be used in this condition because of the poor S/N ratio due to low fluorescence intensity in LiCl-treated animals ($n = 10$ animals). (*E*) Effects of overexpressing *ttx-7* on thermotaxis behavior in adult animals after overnight LiCl treatment. Tukey's multiple comparison test was performed ($n \geq 6$ assays). (*F*) Effects of inositol and other monosaccharides on thermotaxis behavior in adult animals after overnight LiCl treatment. Tukey's multiple comparison test was performed ($n = 4$ assays). (*G*) A model for TTX-7 function. In RIA neurons, the lithium-sensitive enzyme TTX-7/IMPase produces inositol. A supply of inositol is necessary for regulating localization of synaptic components and possibly other cellular functions in mature RIA neurons that together enable the neurons to function as major integrative interneurons for *C. elegans* behavior.

calization recovered considerably after removal of LiCl from the cultivation media (Fig. 7B–D). These results suggest that inhibition of TTX-7/IMPase by lithium in the adult stage causes reversible defects in protein localization and behavior similar to those seen in *ttx-7* mutants, which further supports the hypothesis that these defects are not of irreversible developmental origin.

Lithium chloride exerts its effects by inhibiting TTX-7 in RIA

We next hypothesized that, if LiCl exerts its effects by inhibiting TTX-7, antagonistic treatments should reverse the effects. Thus, we conducted the following experiments using overnight LiCl treatment of adult animals to investigate the effects on the mature nervous system. First, we asked whether overexpression of *ttx-7* could confer LiCl resistance in wild-type animals. As shown in Figure 7E and Supplementary Figure S5H, wild-type animals overexpressing the *ttx-7* genomic clone showed almost normal thermotaxis even after LiCl treatment. In addition, overexpression of *ttx-7a* cDNA specifically in RIA neurons conferred weaker but significant LiCl resistance, which was abolished by increasing the LiCl concentration in the cultivation media (Supplementary Fig. S5I). These results indicate that LiCl exhibits its effect by inhibiting TTX-7 in RIA neurons.

Given the above result, LiCl might cause inositol depletion as well. After being grown with inositol or other monosaccharides to adulthood, wild-type animals were treated overnight with LiCl before the thermotaxis assay. Despite LiCl treatment, the animals grown with inositol showed improved performance (Fig. 7F; Supplementary Fig. S5H). Although sorbitol also improved thermotaxis behavior, this effect was weaker than that of inositol. These results suggest that LiCl affects thermotaxis by inositol depletion. The weaker effect of sorbitol might derive from incomplete inhibition of TTX-7/IMPase by LiCl, which would allow synthesis of inositol from the large amount of sorbitol administered.

Because both *ttx-7* overexpression in RIA neurons and exogenous inositol conferred LiCl resistance, it is conceivable that LiCl perturbs thermotaxis by preventing TTX-7/IMPase from producing inositol in RIA neurons, which is also important for synaptic protein localization (Fig. 7G). Although LiCl reportedly perturbs neuronal polarity in hippocampal neurons by inhibiting GSK-3β, another molecule known for its LiCl sensitivity (Jiang et al. 2005), localization of SNB-1 was intact in RIA neurons of *gsk-3 (tm2223)* mutants (Supplementary Fig. S2A). This excludes the possibility that GSK-3 is the target of LiCl in the process of SNB-1 mislocalization in RIA neurons of *C. elegans*.

Discussion

Loss of TTX-7/IMPase causes specific defects in RIA interneurons

Although *ttx-7* mutants are healthy and reproduce well with slightly reduced brood size, they exhibit severe defects in sensory behaviors, for which the function of RIA neurons is essential (Fig. 2). Despite these limited defects, we could isolate *ttx-7* mutants by forward genetics owing to the vulnerability of the thermotaxis system, which depends on a delicate counterbalance between thermophilic and cryophilic pathways (Fig. 2C). The dispensable nature of TTX-7/IMPase is consistent with the lack of a phenotype in knockout mutants of IMPases in yeast (Lopez et al. 1999). In *C. elegans*, the regulation of inositol trisphosphate signaling is essential for ovulation and defecation (Clandinin et al. 1998; Dal Santo et al. 1999). The mild or absent phenotype of these traits in *ttx-7* mutants indicates that TTX-7/IMPase is not required for all inositol signaling and that *C. elegans* may thus have other inositol-producing enzymes, as is the case in *Dictyostelium* (Van Dijken et al. 1996). The sensitivity of the thermotaxis assay system and the functional specificity of TTX-7/IMPase together make *C. elegans* a unique tool to investigate the function of IMPase in vivo.

In contrast to the severe synaptic localization defects in RIA neurons of *ttx-7* mutants and LiCl-treated wild-type animals, we could not find any significant mislocalization of synaptic proteins in other neurons (Supplementary Fig. S6). The lack of localization defects in neurons in general is consistent with the previous report that knockdown of TTX-7 using RNAi produced no detectable defects in function of the entire nervous system, especially of the neuromuscular junction (Sieburth et al. 2005). The reason for the RIA-specific defects may be ascribed to the properties of RIA neurons, one of the most notable of which is the large number of chemical synapses. Indeed, RIA neurons have the largest number of chemical synapses in the *C. elegans* nervous system except for synapses in nerve cords, which mainly consist of synapses dedicated to direct control of body movement (Supplementary Table S2; White et al. 1986; Oshio et al. 2003). These numerous synapses might in some way confer upon RIA neurons a stronger dependence on TTX-7/IMPase. For example, high levels of total synaptic activity might cause an accelerated consumption of inositol. Indeed, it has been proposed that the effect of lithium on IMPase can be pronounced in neurons with high activity, because the uncompetitive mode of lithium inhibition of IMPase results in increasing inhibition proportional to the activity of the cell (Berridge et al. 1989). A large number of synapses can also confer lithium sensitivity by other mechanisms such as activity-promoted accumulation of lithium in the neuron (Kabakov et al. 1998). RIA neurons express at least three types of non-NMDA-type ionotropic glutamate receptors, of which GLR-3 and GLR-6 are expressed exclusively in RIA neurons (Brockie et al. 2001). Because non-NMDA receptors conduct lithium as well as sodium (Kabakov et al. 1998), it is possible that a large number of synapses containing many glutamate receptors promote lithium uptake, resulting in a higher concentration of lithium in RIA neurons than in other neurons, similar to the uneven accumulation of lithium in mouse brain (Thellier et al. 1980). Given that *C. elegans* probably has

inositol-producing enzymes other than TTX-7/IMPase as discussed above, dependence of each neuronal subtype on a different enzyme may be an additional reason for the IMPase-dependence of RIA neurons.

TTX-7/IMPase produces inositol to regulate the localization of synaptic components in the mature nervous system

Our present work shows that one of the physiological functions of IMPase is to localize synaptic components in the mature nervous system, at least partially by producing inositol. Because inositol-containing lipids are pivotal regulators of membrane traffic (Cremona and De Camilli 2001), we suspected that defects in membrane trafficking caused by inositol depletion might be the reason for protein mislocalization. Thus we screened the available mutants defective in synaptic membrane cycling or inositol signaling to identify downstream targets of IMPase, but we did not identify mutants with the same range and strength of defects seen in *ttx-7* mutants (Supplementary Table S3; Supplementary Fig. S2A). One of the possible reasons for this negative result is that several inositol-regulated molecules work in parallel to serve as downstream effectors of IMPase to regulate protein localization. If that is the case, mutations in multiple genes may result in the same defects as in *ttx-7* mutants, but this is difficult to prove because of the enormous number of possible combinations of mutations, which is one of the most serious problems in current biology. It is also possible that molecules not related to inositol signaling or membrane cycling are involved in the physiological condition, because inositol is not the sole substrate of IMPase (Parthasarathy et al. 1997).

What is the underlying mechanism of mislocalization? The most fundamental question is whether pre- and post-synaptic regions are correctly differentiated, or polarized, in RIA neurites of *ttx-7* mutants. In the *C. elegans* nervous system, the PAR-related kinase SAD-1 and PDZ domain protein SYD-1 have been reported to act in neuronal polarization (Crump et al. 2001; Hallam et al. 2002). Because *ttx-7*, *sad-1*, and *syd-1* mutants each showed different SNB-1 localization in RIA neurites (Fig. 3C; Supplementary Fig. S2A), the three proteins TTX-7, SAD-1, and SYD-1 should act differently in the polarization process of RIA neurons. Because SNB-1 and SYD-2 did localize to some extent to the correct location (Fig. 3C) and did not make ectopic presynapses in the proximal region in RIA neurites of *ttx-7* mutants (Fig. 3F), the polarity in RIA neurites seems at least partially intact. However, these results do not prove that RIA neurites in *ttx-7* mutants have completely intact polarity because *ttx-7* mutants showed more severe localization defects in RIA neurites than *sad-1* and *syd-1* mutants, which should have neuronal polarization defects. As mentioned above, RIA neurites are clearly separated into three regions: distal presynaptic, intermediate isthmus, and proximal post-synaptic regions (Supplementary Fig. S1A). If physical barriers between these regions prevent diffusion of proteins, as in hippocampal neurons (Nakada et al. 2003), disruption of the barriers can be another possible cause of the localization defects.

All the synaptic proteins examined in this study, including both pre- and post-synaptic components, mislocalized in RIA neurons of *ttx-7* mutants. Although this means that RIA neurons of the mutants have more than simple defects like failure to transport specific types of packets, several lines of evidence imply that the fundamental properties of RIA neurons are correctly established and the transportation system in general is not disrupted. First, RIA neurons of *ttx-7* mutants are morphologically intact overall, which means that molecules necessary for general development and maintenance of cell integrity must be normally transported and function properly. Second, localization defects in adult *ttx-7* mutants can be rescued by transient expression of *ttx-7* (Fig. 5), and defects in wild-type animals treated with lithium can be reversed after lithium removal (Fig. 7A–D). These findings suggest that despite mislocalization of many synaptic components, certain cues remain that indicate the correct position of synapses in RIA neurites. The cues may or may not reside in RIA neurons themselves because RIA neurites appeared correctly positioned and could likely communicate with their synaptic partners. Although an electron microscopic (EM) study of ultrastructure in RIA neurons would provide crucial mechanistic insights about mislocalization, observing a specific neuron in vivo under EM is technically challenging.

In this study, we showed that in RIA neurons—one of the most pivotal interneurons in the *C. elegans* nervous system—IMPase plays an important role in regulating localization of both pre- and post-synaptic proteins, which may correlate with behavior. As there have not been previous reports that loss of IMPase causes detectable phenotypes, analysis of *ttx-7* mutants provides valuable information about IMPase function, especially from the aspect of participation of inositol derivatives in synaptic protein localization. In addition, analysis of *ttx-7* mutants and the mechanism of lithium-induced IMPase inhibition in RIA neurons provides better understanding of lithium action on the nervous system. From the viewpoint of lithium targets, it is interesting that GSK-3β does not participate in polarity establishment and maintenance processes in RIA neurons (Supplementary Fig. S2A), which differs from observations in hippocampal neurons (Jiang et al. 2005). These and future findings will pave the way for clarifying the mechanism of lithium's therapeutic effects on human patients by confirming or rejecting IMPase as one of the most plausible lithium targets. Future advances in the therapy will be based on concrete knowledge about IMPase function in vivo, which until now has been completely lacking.

Materials and methods

Strains and genetics

C. elegans culture was essentially as described by Brenner (1974). The following strains were used: wild-type Bristol strain (N2), wild-type Hawaiian strain (CB4856) for mapping with the

snip-SNPs method (Wicks et al. 2001), IK575 *ttx-7(nj40)*, IK589 *ttx-7(nj50)*, IK591 *ttx-7(nj51)*, IK656 *tax-6(db60)*, CB47 *unc-11(e47)*, CZ1893 *syd-1(ju82)*, CX5156 *sad-1(ky289)*, *gsk-3(tm2223)*, and many transgenic strains derived from them. *ttx-7(nj40)* was originally isolated from a genetic screen for associative-learning-defective mutants (Mohri et al. 2005; I. Mori, unpubl.). Deletion mutants *ttx-7(nj50)* and *ttx-7(nj51)* were isolated by the TMP/UV method (Gengyo-Ando and Mitani 2000) with a slight modification in that a mercury lamp attached to an Axioplan2 microscope (Carl Zeiss) was used as the UV source (N. Nishio, H. Inana, and I. Mori, unpubl.). Absence of intact *ttx-7* was verified by PCR. The isolated *ttx-7* mutants were backcrossed to N2 animals 10 times before the analyses.

Behavioral assays

Animals were grown at 20°C, except for the thermotaxis assay in which animals were cultivated at 17°C or 25°C (Supplementary Fig. S3A). The procedure for the thermotaxis assay was as previously reported (Mori and Ohshima 1995), and 20 animals were assayed for each condition in each assay. Except for the assays in Figure 2E and Supplementary Figure S3, the fraction of animals that moved to the 20°C (cultivation temperature) region was calculated. Chemotaxis to odorants was assayed as described by Bargmann et al. (1993), except we used slightly different medium (2% agar, 1 mM $MgSO_4$, 1 mM $CaCl_2$, 25 mM potassium phosphate at pH 6). The dilutions of odorants with ethanol were 1:1000 for diacetyl, 10 mg/mL for pyrazine, 1:100 for isoamyl alcohol, and 1:200 for benzaldehyde. The chemotaxis assay to NaCl was as described (Komatsu et al. 1996). The aldicarb-resistance assay was performed with NGM plates containing 1 mM aldicarb (Wako) as described by Nurrish et al. (1999). Measurements of brood size and defecation cycle were performed as described by Dal Santo et al. (1999), and counting bends was performed as described by Segalat et al. (1995).

Molecular biology

The *ttx-7* genomic sequence including 0.5 kb of the promoter region was amplified from the N2 genome by PCR and cloned to make pTAN3 (*ttx-7*::*EGFP* in Fig. 2A; EGFP amplified from pEGFP-N1; Takara Bio). *ttx-7*a cDNA was amplified from yk808d3 and cloned into pPD49.26 to generate pTAN10. *ttx-7*a from pTAN10 was inserted into each promoter construct to generate specific promoter::*ttx-7*a plasmids. Specific promoters are *gcy-8p* for AFD, *odr-1p* or *str-2p* for AWC, *ttx-3p* for AIY, and *glr-3p* or *glr-6p* for RIA. *snb-1* from pSB120.65 (Nonet 1999) (*snb-1*::*gfp*) and *venus* from yc2.12 (Nagai et al. 2002) were cloned into pTAN41 (*glr-3p*::*gfp*) to obtain pTAN93 (*glr-3p*::*snb-1*::*venus*). *sng-1*::*gfp* from pSY3 (Nonet 1999), *rpm-1*::*gfp* from pCZ161 (Zhen et al. 2000), *gfp*::*syd-2* from pJH23 (Yeh et al. 2005), YFP-GPI (Rolls et al. 2002), and *glr-1*::*gfp* from CR120 (Rongo et al. 1998) were inserted into pTAN41 to make pTAN70 (*glr-3p*::*sng-1*::*gfp*), pTAN111 (*glr-3p*::*rpm-1*::*gfp*), pTAN115 (*glr-3p*::*GFP*::*syd-2*), pTAN134 (*glr-3p*::*YFP*::*GPI*), and pTAN74 (*glr-3p*::*glr-1*::*gfp*), respectively. pTAN135 (*glr-3p*::*snb-1*::*ECFP*) was created by cloning ECFP from pECFP-N1 (Takara Bio) into pTAN93 in place of VENUS. pTAN117 [*glr-3p*::*snb-1(M38A)*::*VENUS*] and pTAN119 [*ttx-7(D99N)*::*EGFP*] were generated by site-directed mutagenesis of pTAN93 and pTAN3, respectively, according to published reports (Atack et al. 1995; Grote and Kelly 1996). Details of all procedures are available upon request.

Transgenic animals

Germline transformation was performed by coinjecting test DNA (1–50 ng/μL) and an injection marker pKDK66 (*ges-1p*::*NLS-GFP*), *ofm-1p*::*GFP*, or pRF4 (*rol-6gf*) into the gonad (Mello et al. 1991). Multiple independent transgenic lines were established for each test DNA. For comparison of phenotypes on different genetic backgrounds, transgenic arrays were transferred by intercrossing. Integrated arrays were made by TMP/UV mutagenesis of the animals with an extrachromosomal array. Animals at the L4 larval stage were soaked in M9 buffer with 0.033 mg/mL trimethylpsoralen (Wako) for 15 min, then irradiated with 365-nm UV light at 1500 μJ/cm^2 using the mercury lamp of an Axioplan2 fluorescence microscope. From their F2 progenies, putative integrants were selected and confirmed by briefly mapping the array using the snip-SNPs method.

Observation and quantification of synaptic molecule localization

Observations were largely performed with an Axioplan2 light microscope. All of the fluorescence images were taken with a confocal laser scanning microscope Fluoview FV500 (Olympus) except for the image in Figure 3F, which was taken with a Fluoview FV1000 (Olympus) for scheduling reasons. The localization index was calculated from confocal images using ImageJ software (NIH). For each optical slice, the area and mean fluorescence intensity of background, the presynaptic region (region A in Fig. 3B), and the rest of the neurite (region B in Fig. 3B) were measured. The total intensity in each region for each slice was calculated by subtracting the mean intensity of background from that of the region of interest, then multiplying the difference by its area. Summing these values for all the slices yielded the "fluorescence" of regions A and B in Figure 3B, from which we generated the localization index from the formula presented there. The A.U. for the amount of SYD-2 described in the text and Figure 7D are equal to the fluorescence intensity of region A calculated in the same way. The fluorescence intensity in cell bodies varied widely among individuals irrespective of genotype and were thus excluded from the calculations. The observations in the last row of Figure 3C (images of GLR-1::GFP) and Supplementary Figures S1D and S2A were performed on animals with integrated arrays, and the others were performed on animals with extrachromosomal arrays.

Application of drugs and heat shock

Drugs were added to cultivation plates. Drugs used were LiCl (15 mM except in Supplementary Fig. S5G,I; Wako), *myo*-inositol (Sigma), sorbitol (Wako), glucose (Wako), and galactose (Sigma). Sugars were used at 200 mM for the thermotaxis assay and at 500 mM for synapse observation. Animals were cultivated on seeded plates containing drugs for the indicated periods before the assay. For inositol rescue experiments in Figure 6, all the animals that were cultivated without inositol were instead cultivated with sorbitol for equivalent osmolarity. Sorbitol did not affect any of the localization or thermotaxis phenotypes of wild-type or *ttx-7* animals (Fig. 6B; data not shown). In Figure 7F, glycerol (Wako) was used as the osmolyte instead of sorbitol because sorbitol affects this assay (Fig. 7F). In heat-shock experiments, animals were cultivated at 30°C for 4 h in the experiments shown in Figure 5, and for the periods indicated in Supplementary Figure S4.

Statistics

Thermotaxis results and localization indexes were treated as parametric and nonparametric data, respectively. When the test methods comparing between only one control group and the others were applied (Dunnett's and Steel's tests), all comparisons are indicated with lines regardless of significance. When other tests were applied, only comparisons with statistical sig-

nificance are indicated with lines. All of the detected statistical significances were indicated with one asterisk for $p < 0.05$ and two asterisks for $p < 0.01$. Error bars in all figures are SEM.

Acknowledgments

We thank C.I. Bargmann for the *odr-1* promoter, CGC for strains, A. Coulson (MRC) for cosmid clones, A. Fire for pPD plasmids, D. Garbars and B. Wedel for the *gcy-8* promoter, Y. Jin for pCZ161, O. Hobert for the *ttx-3* promoter, K.D. Kimura for pKDK66, Y. Kohara for yk clones, A. Miyawaki for yc2.12, National Bioresource Project (Japan) for *gsk-3(tm2223)* mutants, M. Nonet for pSY3 and pSB120, M. Okumura for the *glr-3* and *glr-6* promoters, M. Rolls for YFP-GPI, C. Rongo for CR120, P. Sengupta for *ofm-1p*::*gfp*, P. Swoboda for the *osm-6* promoter, M. Zhen for pJH23, C.I. Bargmann and M. de Bono for helpful suggestions, and Mori laboratory members for fruitful discussions. This work was supported by Grant-in-Aid for Scientific Research on Priority Areas-<Molecular Brain Science>- from the MEXT (00210010) and by HFSPO (to I.M.). I.M. is a Scholar of the Institute for Advanced Research of Nagoya University.

References

Allison, J.H. and Stewart, M.A. 1971. Reduced brain inositol in lithium-treated rats. *Nat. New Biol.* **233:** 267–268.

Arimura, N. and Kaibuchi, K. 2005. Key regulators in neuronal polarity. *Neuron* **48:** 881–884.

Atack, J.R., Broughton, H.B., and Pollack, S.J. 1995. Structure and mechanism of inositol monophosphatase. *FEBS Lett.* **361:** 1–7.

Bargmann, C.I., Hartwieg, E., and Horvitz, H.R. 1993. Odorant-selective genes and neurons mediate olfaction in *C. elegans*. *Cell* **74:** 515–527.

Berridge, M.J., Downes, C.P., and Hanley, M.R. 1989. Neural and developmental actions of lithium: A unifying hypothesis. *Cell* **59:** 411–419.

Brenner, S. 1974. The genetics of *Caenorhabditis elegans*. *Genetics* **77:** 71–94.

Brockie, P.J., Madsen, D.M., Zheng, Y., Mellem, J., and Maricq, A.V. 2001. Differential expression of glutamate receptor subunits in the nervous system of *Caenorhabditis elegans* and their regulation by the homeodomain protein UNC-42. *J. Neurosci.* **21:** 1510–1522.

Clandinin, T.R., DeModena, J.A., and Sternberg, P.W. 1998. Inositol trisphosphate mediates a RAS-independent response to LET-23 receptor tyrosine kinase activation in *C. elegans*. *Cell* **92:** 523–533.

Cremona, O. and De Camilli, P. 2001. Phosphoinositides in membrane traffic at the synapse. *J. Cell Sci.* **114:** 1041–1052.

Crump, J.G., Zhen, M., Jin, Y., and Bargmann, C.I. 2001. The SAD-1 kinase regulates presynaptic vesicle clustering and axon termination. *Neuron* **29:** 115–129.

Dal Santo, P., Logan, M.A., Chisholm, A.D., and Jorgensen, E.M. 1999. The inositol trisphosphate receptor regulates a 50-second behavioral rhythm in *C. elegans*. *Cell* **98:** 757–767.

Dotti, C.G. and Banker, G.A. 1987. Experimentally induced alteration in the polarity of developing neurons. *Nature* **330:** 254–256.

Dotti, C.G., Sullivan, C.A., and Banker, G.A. 1988. The establishment of polarity by hippocampal neurons in culture. *J. Neurosci.* **8:** 1454–1468.

Eisenberg Jr., F. 1967. D-myoinositol 1-phosphate as product of cyclization of glucose 6-phosphate and substrate for a specific phosphatase in rat testis. *J. Biol. Chem.* **242:** 1375–1382.

Gengyo-Ando, K. and Mitani, S. 2000. Characterization of mutations induced by ethyl methanesulfonate, UV, and trimethylpsoralen in the nematode *Caenorhabditis elegans*. *Biochem. Biophys. Res. Commun.* **269:** 64–69.

Gray, J.M., Hill, J.J., and Bargmann, C.I. 2005. A circuit for navigation in *Caenorhabditis elegans*. *Proc. Natl. Acad. Sci.* **102:** 3184–3191.

Grote, E. and Kelly, R.B. 1996. Endocytosis of VAMP is facilitated by a synaptic vesicle targeting signal. *J. Cell Biol.* **132:** 537–547.

Hallam, S.J., Goncharov, A., McEwen, J., Baran, R., and Jin, Y. 2002. SYD-1, a presynaptic protein with PDZ, C2 and rhoGAP-like domains, specifies axon identity in *C. elegans*. *Nat. Neurosci.* **5:** 1137–1146.

Hedgecock, E.M. and Russell, R.L. 1975. Normal and mutant thermotaxis in the nematode *Caenorhabditis elegans*. *Proc. Natl. Acad. Sci.* **72:** 4061–4065.

Jiang, H., Guo, W., Liang, X., and Rao, Y. 2005. Both the establishment and the maintenance of neuronal polarity require active mechanisms: Critical roles of GSK-3β and its upstream regulators. *Cell* **120:** 123–135.

Kabakov, A.Y., Karkanias, N.B., Lenox, R.H., and Papke, R.L. 1998. Synapse-specific accumulation of lithium in intracellular microdomains: A model for uncoupling coincidence detection in the brain. *Synapse* **28:** 271–279.

Komatsu, H., Mori, I., Rhee, J.S., Akaike, N., and Ohshima, Y. 1996. Mutations in a cyclic nucleotide-gated channel lead to abnormal thermosensation and chemosensation in *C. elegans*. *Neuron* **17:** 707–718.

Kuhara, A., Inada, H., Katsura, I., and Mori, I. 2002. Negative regulation and gain control of sensory neurons by the *C. elegans* calcineurin TAX-6. *Neuron* **33:** 751–763.

Lenox, R.H., McNamara, R.K., Papke, R.L., and Manji, H.K. 1998. Neurobiology of lithium: An update. *J. Clin. Psychiatry* **59 (Suppl. 6):** 37–47.

Lopez, F., Leube, M., Gil-Mascarell, R., Navarro-Avino, J.P., and Serrano, R. 1999. The yeast inositol monophosphatase is a lithium- and sodium-sensitive enzyme encoded by a non-essential gene pair. *Mol. Microbiol.* **31:** 1255–1264.

McAllister, G., Whiting, P., Hammond, E.A., Knowles, M.R., Atack, J.R., Bailey, F.J., Maigetter, R., and Ragan, C.I. 1992. cDNA cloning of human and rat brain myo-inositol monophosphatase. Expression and characterization of the human recombinant enzyme. *Biochem. J.* **284:** 749–754.

Mello, C.C., Kramer, J.M., Stinchcomb, D., and Ambros, V. 1991. Efficient gene transfer in *C. elegans*: Extrachromosomal maintenance and integration of transforming sequences. *EMBO J.* **10:** 3959–3970.

Mohri, A., Kodama, E., Kimura, K.D., Koike, M., Mizuno, T., and Mori, I. 2005. Genetic control of temperature preference in the nematode *Caenorhabditis elegans*. *Genetics* **169:** 1437–1450.

Mori, I. and Ohshima, Y. 1995. Neural regulation of thermotaxis in *Caenorhabditis elegans*. *Nature* **376:** 344–348.

Nagai, T., Ibata, K., Park, E.S., Kubota, M., Mikoshiba, K., and Miyawaki, A. 2002. A variant of yellow fluorescent protein with fast and efficient maturation for cell-biological applications. *Nat. Biotechnol.* **20:** 87–90.

Nakada, C., Ritchie, K., Oba, Y., Nakamura, M., Hotta, Y., Iino, R., Kasai, R.S., Yamaguchi, K., Fujiwara, T., and Kusumi, A. 2003. Accumulation of anchored proteins forms membrane diffusion barriers during neuronal polarization. *Nat. Cell Biol.* **5:** 626–632.

Nonet, M.L. 1999. Visualization of synaptic specializations in

live *C. elegans* with synaptic vesicle protein–GFP fusions. *J. Neurosci. Methods* **89:** 33–40.
Nonet, M.L., Holgado, A.M., Brewer, F., Serpe, C.J., Norbeck, B.A., Holleran, J., Wei, L., Hartwieg, E., Jorgensen, E.M., and Alfonso, A. 1999. UNC-11, a *Caenorhabditis elegans* AP180 homologue, regulates the size and protein composition of synaptic vesicles. *Mol. Biol. Cell* **10:** 2343–2360.
Nurrish, S., Segalat, L., and Kaplan, J.M. 1999. Serotonin inhibition of synaptic transmission: Gα(0) decreases the abundance of UNC-13 at release sites. *Neuron* **24:** 231–242.
Oshio, K., Iwasaki, Y., Morita, S., Osana, Y., Gomi, S., Akiyama, E., Omata, K., Oka, K., and Kawamura, K. 2003. Database of synaptic connectivity of *C. elegans* for computation. Technical report of Cybernetic *Caenorhabditis elegans* Program, Keio Future, No. 3, Keio University, Japan. http://ims.dse.ibaraki.ac.jp/research/database_en.html.
Parthasarathy, L., Vadnal, R.E., Parthasarathy, R., and Devi, C.S. 1994. Biochemical and molecular properties of lithium-sensitive myo-inositol monophosphatase. *Life Sci.* **54:** 1127–1142.
Parthasarathy, R., Parthasarathy, L., and Vadnal, R. 1997. Brain inositol monophosphatase identified as a galactose 1-phosphatase. *Brain Res.* **778:** 99–106.
Pollack, S.J., Knowles, M.R., Atack, J.R., Broughton, H.B., Ragan, C.I., Osborne, S., and McAllister, G. 1993. Probing the role of metal ions in the mechanism of inositol monophosphatase by site-directed mutagenesis. *Eur. J. Biochem.* **217:** 281–287.
Rolls, M.M., Hall, D.H., Victor, M., Stelzer, E.H., and Rapoport, T.A. 2002. Targeting of rough endoplasmic reticulum membrane proteins and ribosomes in invertebrate neurons. *Mol. Biol. Cell* **13:** 1778–1791.
Rongo, C., Whitfield, C.W., Rodal, A., Kim, S.K., and Kaplan, J.M. 1998. LIN-10 is a shared component of the polarized protein localization pathways in neurons and epithelia. *Cell* **94:** 751–759.
Segalat, L., Elkes, D.A., and Kaplan, J.M. 1995. Modulation of serotonin-controlled behaviors by Go in *Caenorhabditis elegans*. *Science* **267:** 1648–1651.
Shaldubina, A., Agam, G., and Belmaker, R.H. 2001. The mechanism of lithium action: State of the art, ten years later. *Prog. Neuropsychopharmacol. Biol. Psychiatry* **25:** 855–866.
Sieburth, D., Ch'ng, Q., Dybbs, M., Tavazoie, M., Kennedy, S., Wang, D., Dupuy, D., Rual, J.F., Hill, D.E., Vidal, M., et al. 2005. Systematic analysis of genes required for synapse structure and function. *Nature* **436:** 510–517.
Thellier, M., Wissocq, J.C., and Heurteaux, C. 1980. Quantitative microlocation of lithium in the brain by a (n, α) nuclear reaction. *Nature* **283:** 299–302.
Van Dijken, P., Bergsma, J.C., Hiemstra, H.S., De Vries, B., Van Der Kaay, J., and Van Haastert, P.J. 1996. *Dictyostelium discoideum* contains three inositol monophosphatase activities with different substrate specificities and sensitivities to lithium. *Biochem. J.* **314:** 491–495.
White, J.G., Southgate, E., Thomson, J.N., and Brenner, S. 1986. The structure of the nervous-system of the nematode *Caenorhabditis elegans*. *Philos. Trans. R. Soc. Lond. B Biol. Sci.* **314:** 1–340.
Wicks, S.R., Yeh, R.T., Gish, W.R., Waterston, R.H., and Plasterk, R.H. 2001. Rapid gene mapping in *Caenorhabditis elegans* using a high density polymorphism map. *Nat. Genet.* **28:** 160–164.
Yeh, E., Kawano, T., Weimer, R.M., Bessereau, J.L., and Zhen, M. 2005. Identification of genes involved in synaptogenesis using a fluorescent active zone marker in *Caenorhabditis elegans*. *J. Neurosci.* **25:** 3833–3841.
Zhen, M., Huang, X., Bamber, B., and Jin, Y. 2000. Regulation of presynaptic terminal organization by *C. elegans* RPM-1, a putative guanine nucleotide exchanger with a RING-H2 finger domain. *Neuron* **26:** 331–343.